TOWARD ADVANCING GROUND MOTION MODEL PREDICTIONS FOR THE SIERRAS REGION IN EASTERN CALIFORNIA

Santosh Katuwal[1], Renmin Pretell[1], Jeff R. Bayless[2], Ramin Motamed[1], and Norman A. Abrahamson[3]

[1] Department of Civil and Environmental Engineering, University of Nevada, Reno
[2] AECOM
[3] Department of Civil and Environmental Engineering, University of California, Berkeley

Abstract

We examine the applicability of the Bayless and Abrahamson (2019) effective amplitude spectrum ground motion model (BA18) for the Sierras region of Eastern California. An overall tendency to overpredict low-frequency ground motions, and to underpredict high-frequency ground motions is identified. The over- and underpredictions are due to site condition discrepancies between the stations considered in the BA18 model development, and the Sierras region, namely the velocity structure used in estimating earthquake magnitudes, and the high-frequency attenuation and site amplification patterns. An analysis of site terms shows the potential for including site-specific predictors beyond the time shear-wave velocity (V_S) in the top 30 m (V_{S30}) for BA18 applications in the Sierras.

Introduction

Assessing seismic demands is critical in the seismic design of infrastructure. Ground-motion models (GMMs) are commonly used for quantifying ground motions as a function of earthquake source characteristics, wave-propagation paths, and local site conditions. Over the past two decades, significant advances in empirical GMMs have been made through coordinated efforts such as the Next Generation Attenuation (NGA) projects. The NGA West 2 (NGA-West2) project provides the most recent set of NGA GMMs for active crustal regions. These GMMs provide first-order ground motion estimates for seismic hazard assessments in California. However, their accuracy can be limited in areas that are overall poorly represented by the data used in GMM developments, such as the Sierras region of Eastern California.

The Sierras region presents geological conditions that differ in stiffness and quality from those in Western California. The Sierras region is delimited based on geological maps, and a digital elevation model. The geological maps are used to identify the extent of the mountains, with the western margin following the contact with the Central Valley and the eastern margin aligned with the major faults that mark the transition to the Basin and Range physiographic province. The Sierras region is distinguished by extensive exposures of the granitic Sierras Nevada Batholith, surrounded by metamorphic belts, and bounded to the west by the sedimentary deposits of the Great Valley and to the east by the extensional Basin and Range province (Bateman 1992, Unruh 1991). The digital elevation model is then used as a reference to

refine these limits based on the high-elevation uplands and the slopes along the eastern side of the range. The range is defined by a broad, gentle slope descending into the Central Valley along its western margin, contrasted with a steep normal-fault escarpment to the east, reflecting cumulative late Cenozoic uplift and tilt (Huber 1981). Together, these datasets provide a consistent definition of the Sierras region, extending across the California-Nevada border, shown in Figure 1.

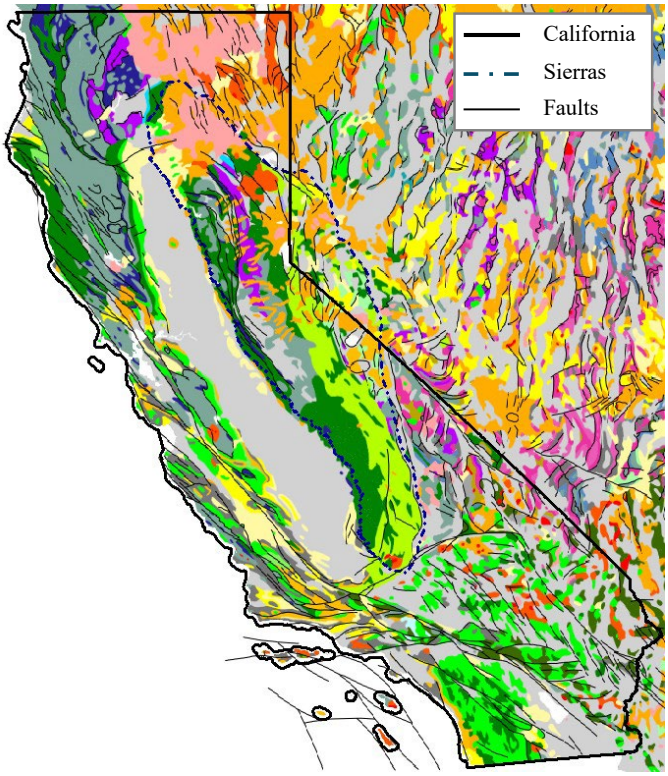

Figure 1. Geologic map of California showing the delineated Sierras region. Major fault systems are shown as thin black lines, highlighting the structural framework that defines the Sierras region (King et al. 1974).

Bayless and Abrahamson (2019) developed a GMM for effective amplitude spectra (EAS) (Goulet et al. 2018) using NGA-West2 data, dominated by data from Western California. Western California predominantly consists of coastal and basin environments with thick sedimentary sequences and low-V_S deposits. In contrast, the Sierras presents lower attenuation and more pronounced high-frequency energy retention compared to the Great Valley and Coast Ranges (Eberhart-Phillips 2016, Phillips and Stead 2008). Subsurface conditions define both the path and the site effects captured by GMMs, and it is thus expected that ground motion estimates based on the BA18 GMM might be biased when applied to locations in the Sierras region. Figure 2 shows the data used to develop the BA18 GMM, differentiating the recordings collected within the Sierras.

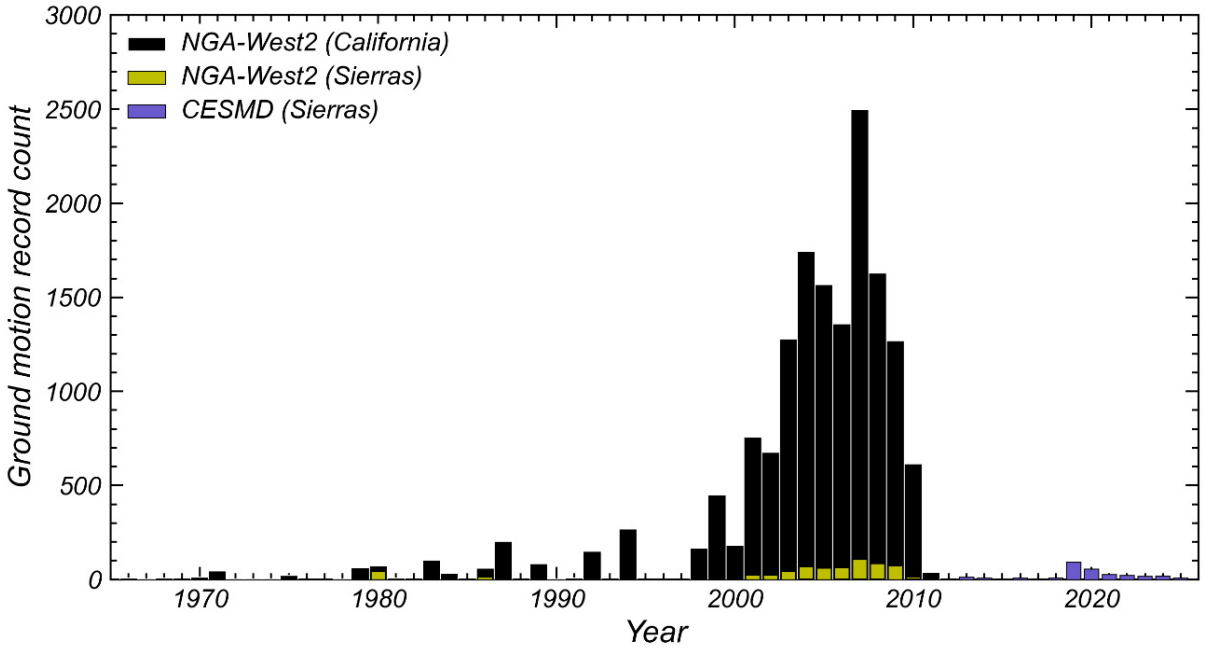

Figure 2. Annual distribution of recorded earthquake events in the NGA-West2 dataset, used to develop the Bayless and Abrahamson (2019) ground motion model, and the data used in this study for the Sierras region in Eastern California.

In this study, we assess the applicability of the Bayless and Abrahamson (2019) GMM, hereafter referred to as BA18, for the Sierras of Eastern California. We also investigate the potential for revising the model for applications in the Sierras, and incorporating site-specific parameters derived from shear-wave velocity (Vs) measurements. The model's performance is assessed by comparing their estimates against recorded ground motions, i.e., residuals. First, a subset of stations in the Sierras region are selected. Ground motion data are downloaded from public datasets, and the EAS computed. The residuals are calculated and partitioned into event, site, and within-site components using mixed-effects regressions at individual frequencies, and trends between site terms and Vs-based parameters investigated. Our results indicate that the BA18 GMM leads to an overall overprediction of EAS ordinates at low frequencies, up to about 2 Hz, and an overall underprediction for frequencies higher than 3 Hz. This bias, the between-event, between-site, and within-site standard deviations, and the potential for incorporating site-specific parameters to the BA18 GMM for applications in the Sierras region are discussed.

Ground motion and site data

Twelve ground motion stations within the Sierras region (Figure 1) are selected based on the availability of neighboring measured Vs profiles. In this section, we discuss the ground motion and site data for these stations, emphasizing the aspects that differ from the NGA-West2 data used by Bayless and Abrahamson (2019).

Recorded ground motion

Ground motion data recorded at the selected stations, provided by the California Strong Motion Instrumentation Program (CSMIP), are downloaded in processed form (i.e., *.V2 format) from the Center for Engineering Strong Motion Data (CESMD). The data consist of three-component accelerograms recorded at the selected seismic stations during shallow crustal earthquakes with **M**3 or larger. Only the data from earthquakes recorded at three or more ground motion stations are retained, criteria that leaves a total of 266 two-component recordings. The ground motion metadata, such as earthquake magnitude (**M**), hypocentral depth (Z_{hyp}), and epicentral coordinates, are provided by CESMD. Ground motion processing details are also provided, including filter frequencies, baseline correction information, and unit conventions.

The recordings are used to compute EAS ordinates, which serve as the primary ground motion intensity measure used in this study. The EAS are computed by combining the Fourier amplitude spectra of the horizontal components using Eq. 1.

$$EAS = \sqrt{\frac{FAS_{H1}^2 + FAS_{H2}^2}{2}} \quad (1)$$

where FAS_{H1} and FAS_{H2} are the Fourier amplitude spectra of the two horizontal recorded components. Consistent with Bayless and Abrahamson (2019), the resulting EAS is smoothed using the Konno and Ohmachi (1998) smoothing window, b = 40.

The annual distribution of earthquakes recordings included in the NGA-West2 dataset, used by Bayless and Abrahamson (2019), and our dataset is shown in Figure 2. The NGA-West2 dataset consists of over 21 thousand two-component recordings recorded up to around 2010, and includes recordings of several important earthquakes in California, and other active crustal regions. In contrast, our dataset for the Sierras region consist of 266 two-component recordings that are primarily collected after 2015. Highlighted in Figure 2 is also the distribution of the 613 NGA-West2 recordings located within the Sierras region. Only 6 recordings are common for both the NGA-West2 and our dataset as we have selected stations based on the availability of a measured V_S profile, whereas the NGA-West2 dataset incorporates stations with proxy-based time-average V_S in the uppermost 30 m (V_{S30}). This figure suggests an important underrepresentation of the Sierras region in the NGA-West2 dataset, which is therefore inherent to BA18 GMM.

The distribution of data in terms of earthquake magnitude and epicentral distance is presented in Figure 3. As observed, the NGA-West2 dataset (Figure 3, left panel) spans a wide range of epicentral distances between 1 to 300 km, for **M**3 to **M**5 events, but the range narrows down for larger magnitude events. Similarly, most recordings in our dataset (Figure 3, right panel) are concentrated in the **M**3.5 to **M**5.5 range, with epicentral distances within a narrower range from 3 to 100 km. Specifically for the Sierras, our dataset has a denser presence of low magnitude events (**M**3 to **M**4) and intermediate epicentral distances, between 10 and 50 km, as well as a very limited but richer presence of recordings corresponding to large magnitude events recorded at long distances.

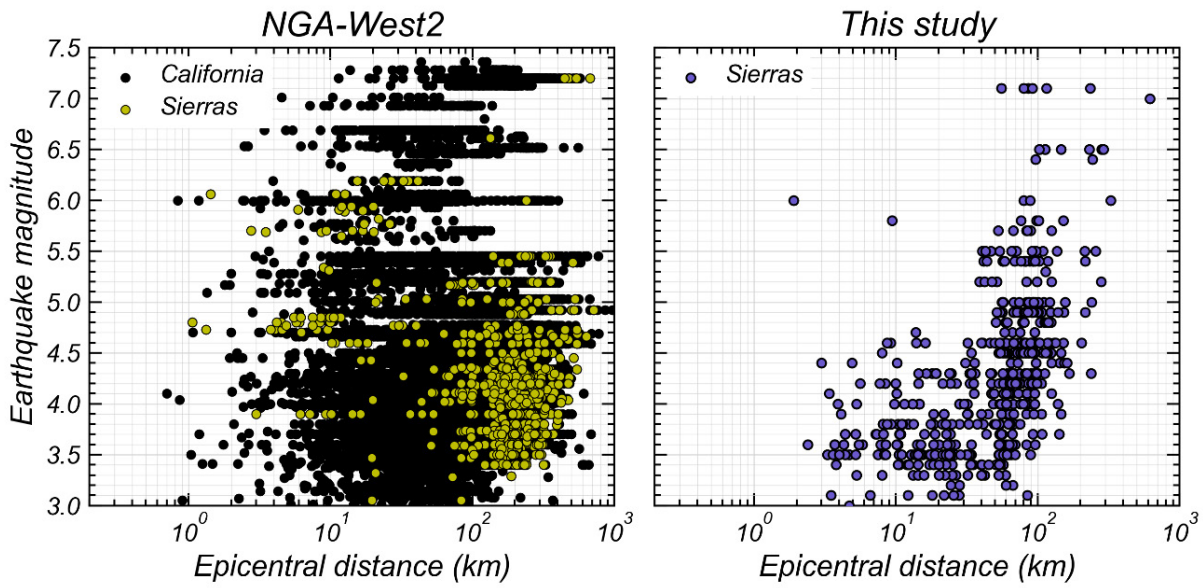

Figure 3. Earthquake magnitude versus epicentral distance pairs for (a) NGA-West2 dataset, and (b) the dataset collected for this study.

Ground motion stations

As part of this study, we aim to identify site-specific parameters with ground motion predicting ability that could be incorporated into the BA18 GMM for application in the Sierras region. Thus, the site characterization consists of measured V_S profiles. Twelve stations with a measured V_S profile available within a radius of 200 m are selected. This radius is selected as a compromise between the number of stations available, and the closeness of the V_S profile. The available V_S profiles are accessed through the V_S Profile Database (VSPDB) by Ahdi et al. (2018). The profiles collected are derived from a combination of measurements, including downhole and suspension logging, cone penetration testing, and surface-wave measurements. Each profile includes layer thickness and velocity information that enable computation of V_{S30} and other site-specific predictions, discussed later in this paper.

Figure 4 presents the Vs profiles for our twelve stations within the Sierras region. These profiles illustrate the variation in near-surface velocity structure across different geological settings of the range. The stations CE54933 and CE54517 share the same V_S profile because they are located within 200 m of the same VSPDB site. The stations CISPG2, CICWC, and CITEH show relatively high V_{S30} values and steep velocity gradients (i.e., rapid increase in V_S with depth), reflecting stiffer near-surface conditions and shallow impedance contrasts. Meanwhile, the stations CE54933 and CIMLAC exhibit lower V_S and milder gradients, indicative of softer, deeper sediments. The depth of the largest velocity jump varies from only a few meters at some stations to depths exceeding 100 m at others, suggesting differences in the dominant frequency range of site amplification. Collectively, these variations demonstrate the diverse near-surface conditions for the Sierras region.

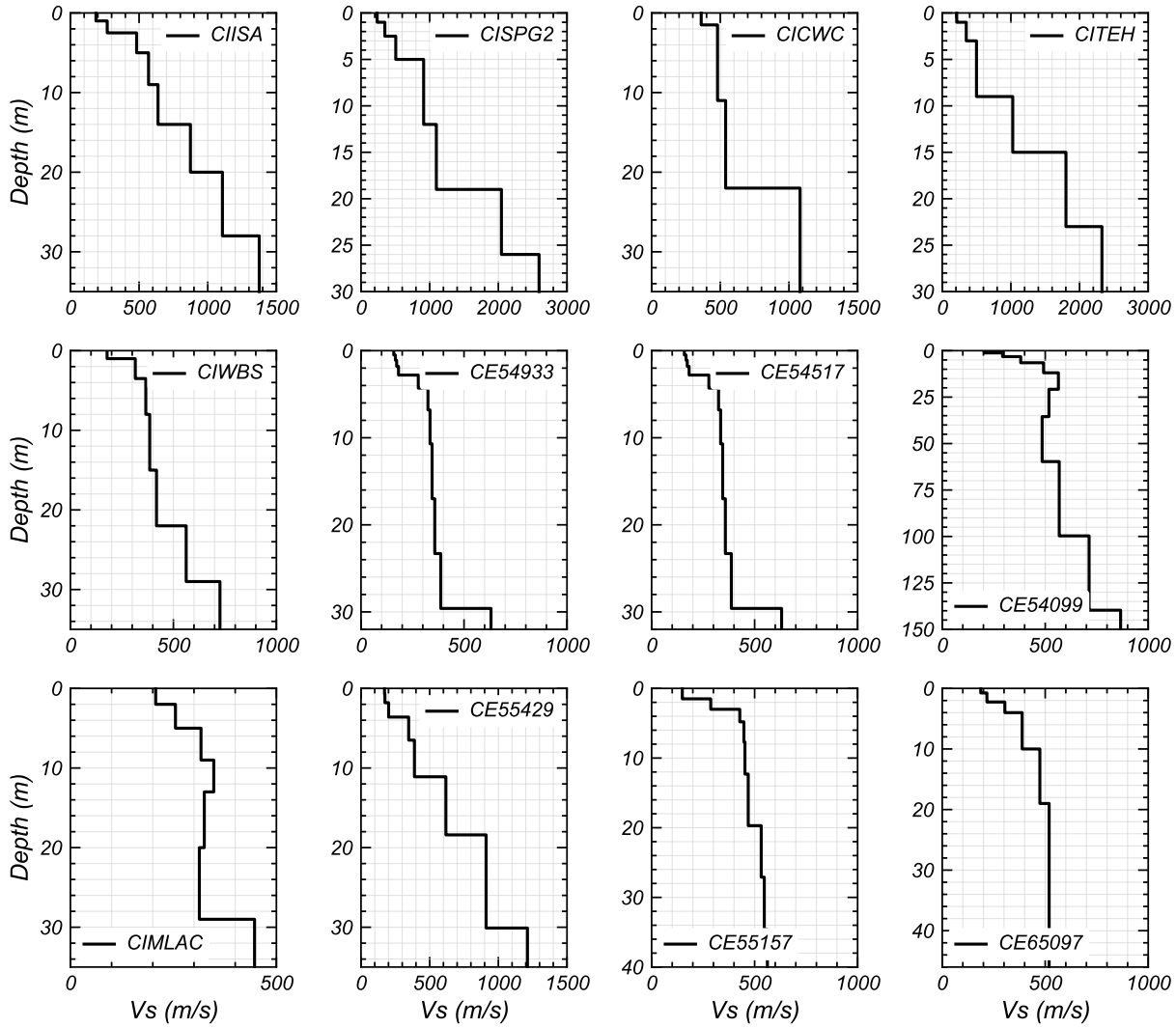

Figure 4. Shear-wave velocity (Vs) profiles for the twelve stations used in this study.

An additional parameter required is the site-to-source distance. Specifically, we need rupture distances (R_{rup}) as this is an input of the BA18 GMM. Our dataset for the Sierras is based on CESMD data, with small-to-moderate earthquake magnitude events (Figure 3b), which do not have finite fault models readily available. Thus, we use the ps2ff Python library to convert point source distance measures into average R_{rup} values. The ps2ff library follows the methodology described by Thompson and Worden (2018) to estimate R_{rup} based on epicentral (R_{epi}) or hypocentral distances, and Z_{hyp}, based on numerical integration across probability distributions that represent seismological constraints on rupture geometry. Rupture area is first estimated from earthquake magnitude using established magnitude-area scaling relations (Hanks and Bakun 2008, Wells and Coppersmith 1994). The variability in strike, dip, and hypocentral position is then incorporated to generate statistical estimates of mean R_{rup} conditioned on R_{epi} and **M**.

Performance assessment of the BA18 GMM for the Sierras

The BA18 GMM's performance for estimating ground motions is assessed based on the residuals obtained for the Sierras, focusing on two aspects. First, any biases observed in residuals across frequencies, and with site-to-source distance. Second, the magnitude of the residuals relative to those obtained during the BA18 GMM development. The BA18 model requires earthquake source, path, and site parameters to estimate median ground motions. The model parameters include moment magnitude (**M**), rupture distance (R_{rup}), depth to top of rupture (Z_{tor}), style of faulting, time averaged shear wave velocity in the upper 30 m (V_{S30}), and basin depth proxy (Z_1). The GMM functional form is shown in Eq. 2.

$$\ln(EAS) = f_M + f_P + f_S + f_{Ztor} + f_{NM} + f_{Z1} \tag{2}$$

where f_M, f_P, f_S, $f_{Z_{tor}}$, f_{NM}, and f_{Z_1} are terms that capture the scaling due to magnitude, path, site response, depth to top-of-rupture, style of faulting, and soil depth. The BA18 implementation in the pygmm Python library (Kottke et al. 2025) is used.

Residuals

Residuals are defined as the difference between observed and GMM-based (i.e., predicted) ground motions in natural logarithmic units, as shown in Eq. 3.

$$R_{ij} = \ln\left(Y_{ij}\right) - \ln\left(\hat{Y}_{ij}\right) \tag{3}$$

where Y_{ij} is recorded EAS measure for an event "i" at a site "j," while $\hat{Y}_{ij}$ denotes the GMM-based median EAS counterpart. Negative residuals indicate overprediction of the median GMM prediction, whereas positive residuals indicate underprediction. Eq. 3 is applied to our dataset for the Sierras for several frequencies ranging from 0.4 to 25 Hz. The lower limit of 0.4 Hz is the minimum usable frequency with at least 40 recordings across the entire dataset.

The total residuals estimated using Eq. 3 are then partitioned to observe the contributions from the deviations of both the event and site BA18 scaling terms, and the remaining within-site residual variability. These components are partitioned using linear mixed-effects regressions based on Eq. 4, where c_1 is the method bias in the GMM when applied to the Sierras region, η_i is the event term, S_j is the site term, and ε_{ij} is the remaining within-site residual.

$$R_{ij} = c_1 + \eta_i + S_j + \varepsilon_{ij} \tag{4}$$

The event term is also represented as δB and referred to as between-event residual. The site term is also represented as $\delta S2S$ and referred to as between-site residual. The random effects are assumed to be normally distributed with variances τ^2 for the event terms, and ϕ_{S2S}^2 for the site terms, while the variance ε_{ij} represents single station variability ϕ_{SS}^2. The mixed-effects regressions are conducted using the Python library statsmodel (Seabold and Perktold 2010).

Observed trends

The variation of residuals across frequencies for all 266 EAS in our dataset for the Sierras is presented in Figure 5. Each gray line corresponds to a recording in our dataset. A wider spread of residuals is observed at low frequencies, which narrows down at frequencies higher than approximately 4 Hz. Figure 5 also shows the method bias, c_1. The method bias exhibits gradual variation with frequency, with an overall tendency of overprediction at low frequencies, and underprediction at high frequencies. At intermediate frequencies, between 1 and 2 Hz, the residuals are near zero, on average. The peak over- and underprediction observed at about 0.5 and 15 Hz in the method bias is about 0.7 natural logarithmic units. This residual value indicates that, on average, GMM-based EAS could be as high as twice as recorded around 0.5 Hz, and as low as half as recorded around 15 Hz.

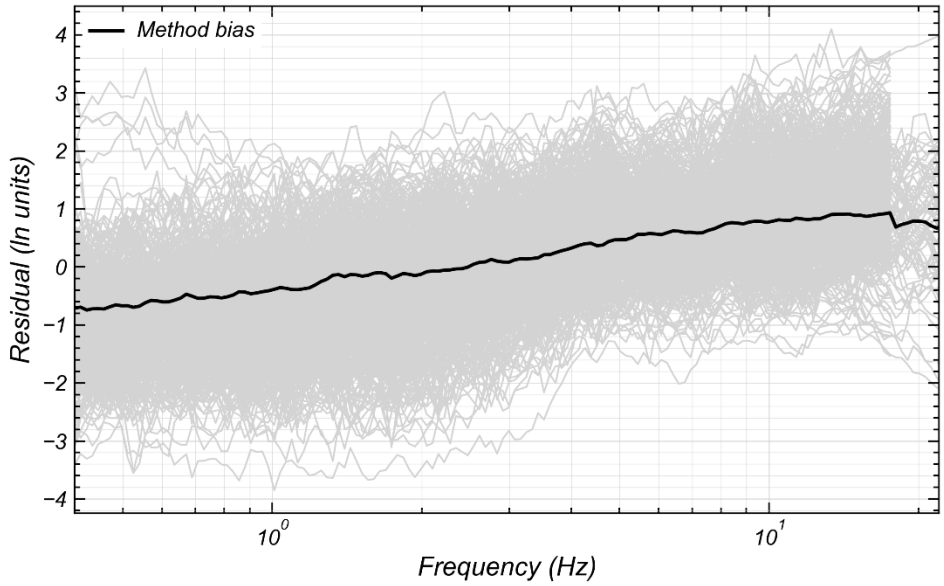

Figure 5. Residuals for effective amplitude spectrum ordinates.

The observed trends of over- and underpredictions at low and high frequencies are explained by physical characteristics of the Sierras. The overpredictions at low frequencies are caused by a bias in the earthquake magnitudes. A recent study by Pinilla-Ramos et al. (submitted) identified a bias in the magnitude values assigned to earthquakes across California. The earthquake magnitudes for events across California are estimated following the same protocols established by the Advanced National Seismic System, however using different velocity structures. The Coastal California regions, approximately north of the San Fernando valley (Los Angeles) uses the Gil7 velocity model (Dreger and Romanowicz 1994), whereas the rest of California except Mendocino, including the Sierras region, uses the SoCal velocity model (Kanamori and Hadley 1975). The Gil7 model is softer near surface compared to the SoCal velocity model. This difference leads to earthquake magnitudes along the coastal regions that are lower than they would have been if estimated using the SoCal velocity model. Analogously, earthquake magnitudes in the Sierras are higher than they would have been if estimated using the

Gil7 velocity model. These tendencies, carried in the ground motion metadata of NGA-West2, are inherent to the BA18 GMM and lead to an overall overprediction of ground motions at low frequencies (negative residuals), and underprediction at high frequencies (positive residuals). This effect is significantly more important at low frequencies as the magnitude scales ground motion amplitudes in a factor of approximately 30 below the earthquake corner frequencies.

The underpredictions at high frequencies are explained by the shallow velocity structure of the Sierras, due to different patterns in the (1) high-frequency site amplification, and (2) high-frequency wave attenuation. First, the Sierras region has areas with sharp impedance contrasts near surface, and relatively shallow rock materials as implied by the V_S profiles in Figure 4 (e.g., CICWC). These site conditions lead to a more pronounced amplification of the high-frequency range. Katuwal and Pretell (2025) conducted a numerical study and demonstrated that near-surface velocity contrasts can significantly increase high-frequency amplification. As the BA18 model was developed based on data from deeper, softer profiles, such high-frequency amplifications are not captured, and rather observed as positive residuals.

Second, rock formations in the Sierras region have higher quality factors than the Western and Southern California, as observed in Figure 6 by Lavrentiadis et al. (2021). Higher quality factors lead to milder wave attenuation, and consequently higher high-frequency ground motions within the Sierras compared to the rest of California. The NGA-West2 dataset used for developing the BA18 GMM is strongly dominated by data collected in areas outside the Sierras region (Figure 1), therefore it has a more rapid wave attenuation of high-frequency waves that is particularly observable at long distances, corresponding to the Sierras region (Figure 3). This trend is also observed in Figure 7, as the residuals tend towards more positive values, indicating underprediction at long R_{rup} and high-frequency EAS.

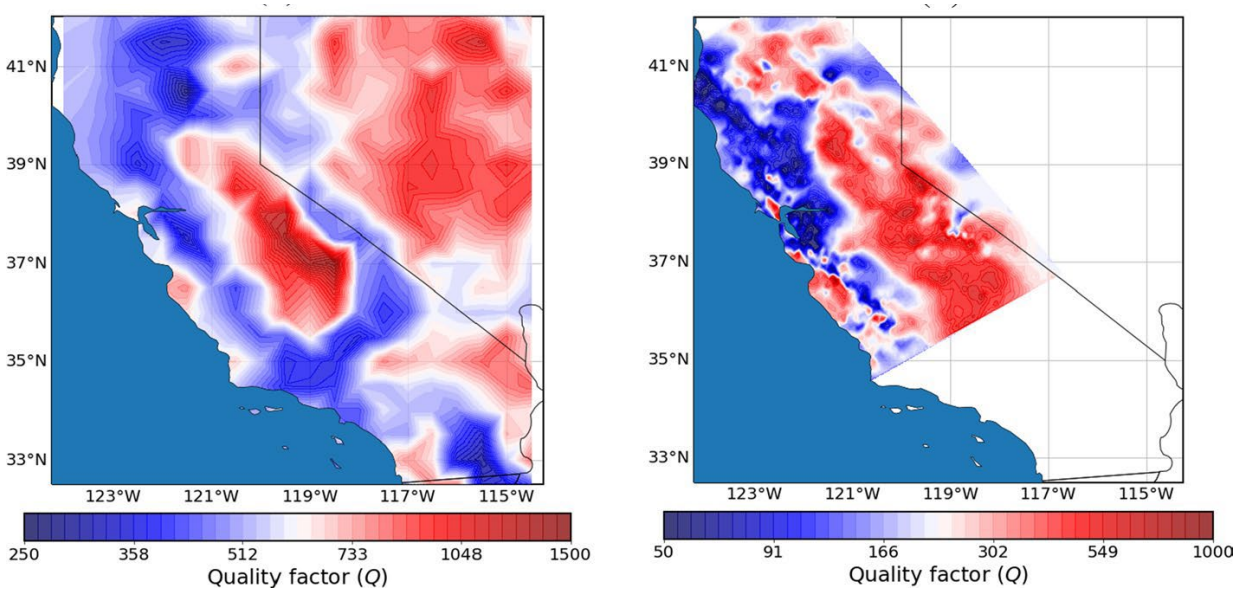

Figure 6. Seismic attenuation models for California: (a) Phillips et al. (2014) attenuation model for frequencies between 6 and 12 Hz, and (b) Eberhart-Phillips (2016) S-wave attenuation model for northern California at a depth of 4 km. Figure by Lavrentiadis et al. (2021).

Histograms of the event and the site terms for the twelve stations used in this study are presented in Figures 8 and 9, respectively, for different frequencies. Based on Figure 8 and results at neighboring frequencies not included herein for brevity, the event terms tend towards more negative values at low frequencies, consistent with the observations by Pinilla-Ramos et al. (submitted). Figure 9 shows a distinctive tendency of near-zero site terms at 7 Hz. The site terms at 0.5, 1, and 15 Hz show positive and negative values without a clear preference and presents a similar scatter as the BA18 site terms (Bayless and Abrahamson 2019). The positive site terms at 15 Hz, indicative of underprediction, correspond to the sites with relatively shallow impedance contrasts (Figure 4). This is consistent with findings by Katuwal and Pretell (2025) regarding sites with shallow impedance contrasts.

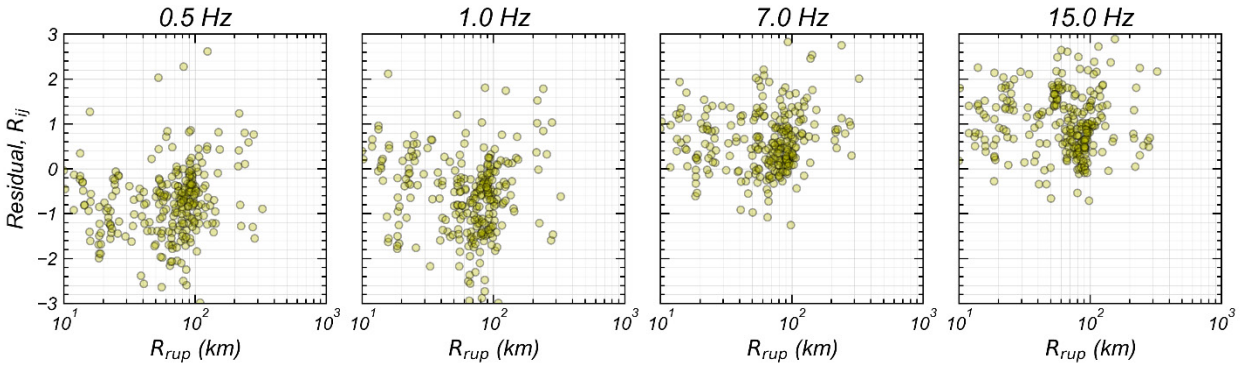

Figure 7. Variation of residuals for the Sierras region with rupture distance.

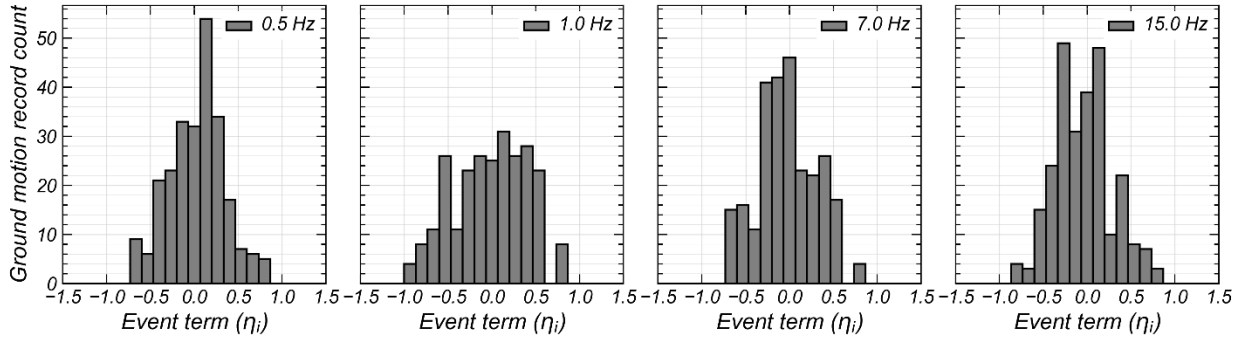

Figure 8. Histogram of event terms at different frequencies for the Sierras region.

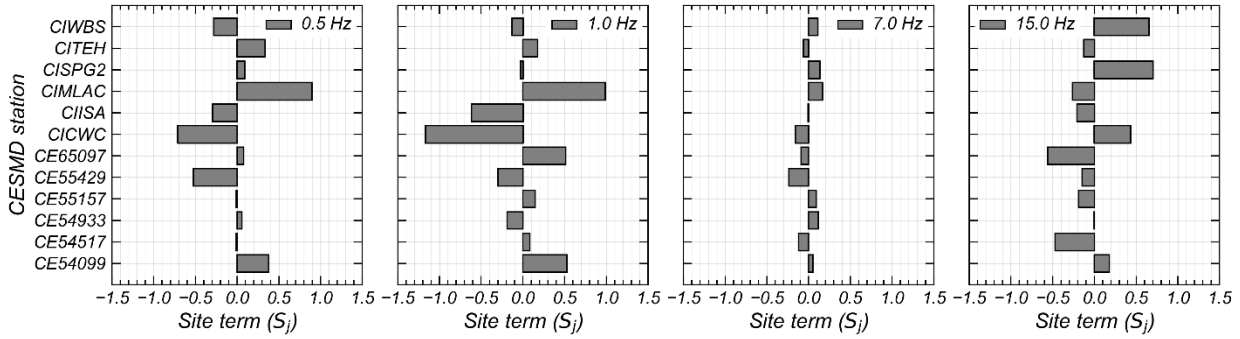

Figure 9. Histogram of site terms at different frequencies for the Sierras region.

The between-event (τ), between-site (ϕ_{S2S}), and within-site (ϕ_{SS}) standard deviations are shown in Figure 10 for the BA18 GMM when applied to the NGA-West2 data used for the model development (left panel), and our study for the Sierras (right panel). The τ for the BA18 GMM and our study varies from about 0.6 at low frequencies, to values between 0.3 and 0.4 at intermediate frequencies, between 2 and 6 Hz. At higher frequencies, the BA18 GMM τ gets back to values around 0.6, whereas τ stays at around 0.35 for the Sierras. A lower τ indicates a more consistent variation of event terms in the Sierras. The ϕ_{SS} is more consistent in both studies, with values ranging from about 0.35 to 0.45 at low frequencies, and a mild tendency to increase at mid frequencies, around 4 Hz. At higher frequencies, ϕ_{SS} continues to increase up to about 0.55 for BA18 and decreases to about 0.4 for the Sierras region at 15 Hz.

A more important difference is observed for the ϕ_{S2S} for BA18's and our dataset. The site-to-site variability is about 0.4 across frequencies up to 4 Hz for BA18 and increases to 0.6 at higher frequencies. Meanwhile, ϕ_{S2S} varies from 0.4 at low frequencies to 0.6 at about 4 Hz for the Sierras. The site-to-site variable then decreases to a minimum between 0.1 and 0.2 within 5 and 8 Hz, and increases back to about 0.6 at about 20 Hz. The ϕ_{S2S} variation observed in the Sierra data emphasizes the influence of localized geological and topographical conditions that deviate from the statewide average observed in the BA18 ϕ_{S2S}.

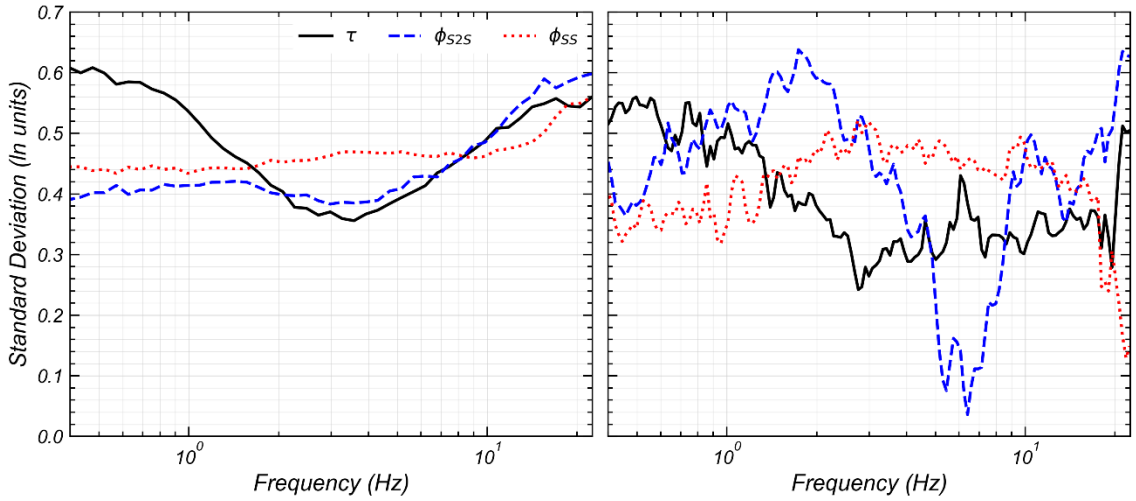

Figure 10. Between-event (τ), between-site (ϕ_{S2S}), and within-site (ϕ_{SS}) standard deviations. (a) Standard deviations for the BA18 GMM, (b) standard deviations calculated in this study.

Site response predictors

The BA18 GMM uses V_{S30} as a proxy for site conditions controlling the first-order site response characteristics of linear and nonlinear site amplification. However, V_{S30} alone cannot fully capture the complexities of near-surface stiffness and impedance structure, particularly in regions with shallow bedrock, strong velocity gradients, or layered crystalline materials, like the Sierras. In this section we study the potential need for a revised V_{S30} scaling for the Sierras, and

the predicting ability of additional site-specific parameters to explain the site terms. Specifically, we study an alternative time-average V_S, namely V_{S10}, and a gradient parameter, g.

The velocity gradient is quantified using Eq. 5, where ΔV_{Sz} is the difference in V_S between the uppermost and bottommost layers in the V_S profile within depth z, and ΔH_z is the change in depth between the middle points of those two layers.

$$g_z = \frac{\Delta V_{Sz}}{\Delta H_z} \tag{5}$$

For example, g_{30} and g_{10} denote the gradient in the top 30 m and 10 m of the Vs profile respectively. These parameters describe the rate of stiffness increase within the near-surface materials and provide a physically meaningful indicator of frequency-dependent amplification. Prior studies have demonstrated that sites with steeper velocity gradients tend to show stronger high-frequency amplification and higher resonant frequencies (Cascone et al. 2022, Katuwal and Pretell 2025, and Régnier et al. 2014). Incorporating these gradient measures alongside the time-averaged velocities enhances the ability to capture localized variations in site response that are not represented by V_{S30} alone.

The variation of site terms for four site-specific parameters, (i.e., predictors) is presented in Figure 11 for 1, 4, and 20 Hz. At 1 Hz (Figure 11, left column), all predictors exhibit a weaker linear relation with the site terms. This behavior was anticipated as the investigated predictors are better suited to capture near-surface site amplification effects, which impact higher frequencies. At 4 Hz (Figure 11, middle column), the correlations become stronger, with an evident negative linear correlation for all parameters. At 20 Hz (Figure 11, right column), the trends shift from negative to positive for all predictors. This reversal indicates that higher-frequency amplification is pronounced at stiffer sites, or sites with stronger velocity gradients.

Conclusions

The applicability of the Bayless and Abrahamson (2019) effective amplitude spectra (EAS) ground-motion model (GMM) for the Sierras region of Eastern California was investigated using 266 earthquake recordings available across twelve ground motion stations. These stations were selected as a neighboring measured shear-wave velocity (V_S) profile measurement was available. The ground motion data were used to compute residuals, and the observed trends were explained by the differing characteristics between the sites used for developing BA18 and the sites in the Sierras. The residuals were partitioned using mixed-effects regressions, and the potential for explaining the site terms using site-specific parameters beyond the common time-average shear wave velocity (V_S) in the top 30 m (V_{S30}) investigated.

We identified an overall tendency of the BA18 GMM to overpredict low-frequency EAS ordinates, and to underpredict the high-frequency range. These over- and underpredictions peaked at 0.5 and 15 Hz, respectively, in a factor of 2, indicating that ground motions estimated near 0.5 Hz can be as high as twice the recorded (on average), and as low as half near 15 Hz. The residuals are near zero, on average, between 1 and 2 Hz. The overprediction at low frequencies was due to the different velocity structure used in estimating earthquake magnitudes in

California. The underprediction at high frequencies was due to the discrepancies in high-frequency attenuation and site amplification patterns between the Sierras and the broader California regions. An investigation of site-specific V_{S30}, the time-average V_S for the top 10 m (V_{S10}), and velocity gradient parameters suggested the potential for revising the V_{S30} scaling of BA18 GMM for applications in the Sierras or incorporating new parameters.

Future work will focus on three aspects, namely (1) the integration of additional ground motion stations within the Sierras region upon availability of newly measured shallow V_S profiles, (2) the investigation of additional site-specific V_S-related predictors, and (3) the development of adjustment relationships for applications of the BA18 model in the Sierras region of Eastern California.

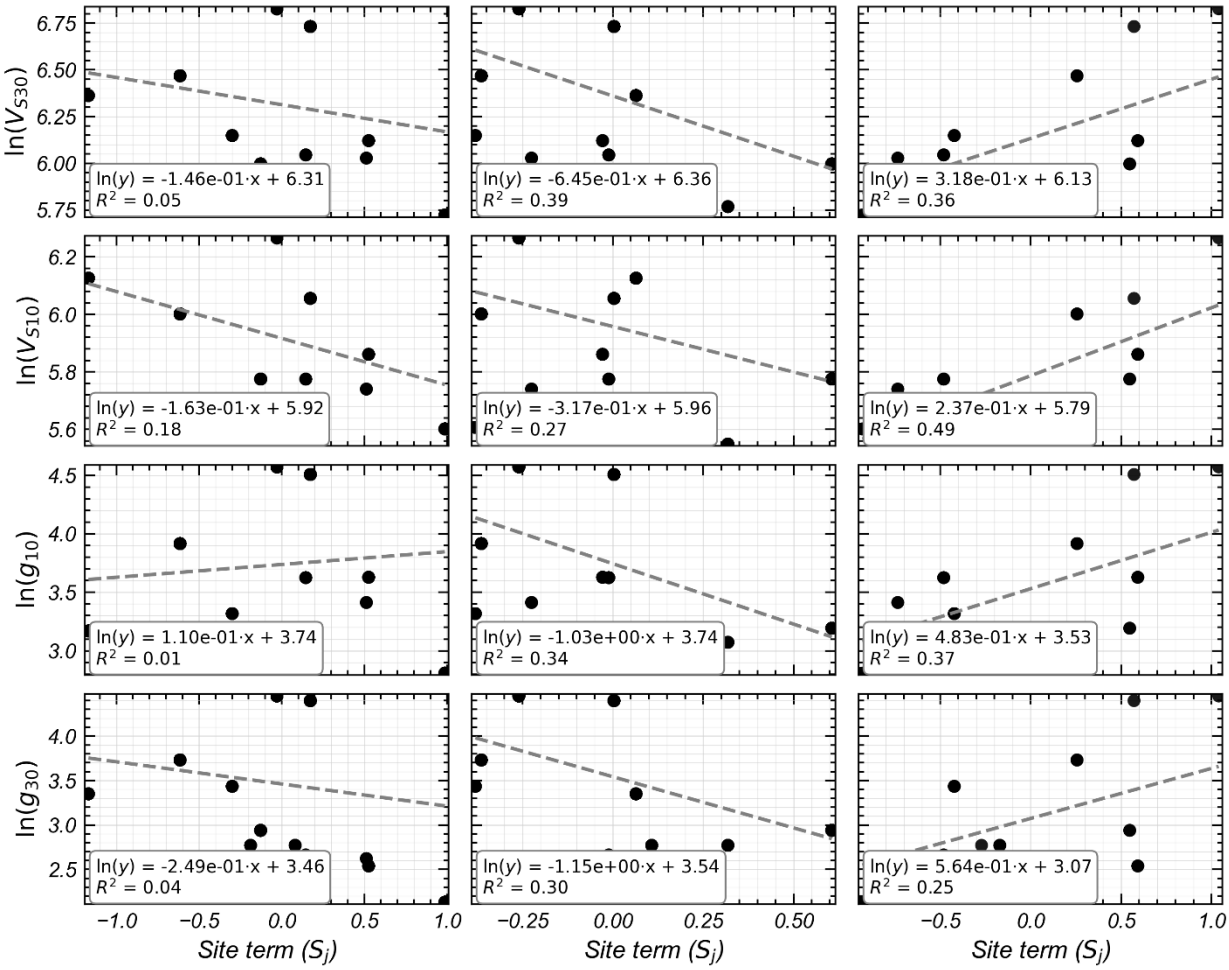

Figure 11. Relationships between site terms and time-average V_S and V_S gradient (g) predictors. Each subplot includes a linear regression fit (dashed line).

References

Ahdi SK, Sadiq S, Ilhan O, et al. (2018) Development of a United States community shear wave velocity profile database. *Geotechnical Earthquake Engineering and Soil Dynamics V*. American Society of Civil Engineers Reston, VA, pp.330-339.

Ancheta TD, Darragh RB, Stewart JP, et al. (2014) NGA-West2 database. *Earthquake Spectra* 30(3): 989-1005.

Bateman PC (1992) *Plutonism in the central part of the Sierra Nevada batholith, California.* US Government Printing Office.

Bayless J and Abrahamson NA (2019) Summary of the BA18 ground-motion model for Fourier amplitude spectra for crustal earthquakes in California. *Bulletin of the Seismological Society of America* 109(5): 2088-2105.

Campbell KW and Bozorgnia Y (2019). Ground motion models for the horizontal components of Arias Intensity (AI) and Cumulative Absolute Velocity (CAV) using the NGA-West2 database. *Earthquake Spectra*, 35(3), 1289–1310.

Cascone V, Barone I and Boaga J (2022) Velocity gradients choice affecting seismic site response in deep alluvial basins: Application to the Venetian Plain (Northern Italy). *Journal of Geophysics and Engineering* 19(1): 1–13.

Dreger DS and Romanowicz B (1994) Source Characteristics of Events in the San Francisco Bay Region. *Technical Report Open-File Report* 94-176, U.S. Geological Survey. ISSN: 2331–1258.

Eberhart-Phillips D (2016) Northern California seismic attenuation: 3D QP and QS models. *Bulletin of the Seismological Society of America* 106(6): 2558-2573.

Goulet C, Kottke A, Boore D, et al. (2018) Effective amplitude spectrum (EAS) as a metric for ground motion modeling using Fourier amplitudes. *2018 Seismology of the Americas Meeting.*

Hanks TC and Bakun WH (2008) M-log A observations for recent large earthquakes. *Bulletin of the Seismological Society of America* 98(1): 490-494.

Huber NK (1981) *Amount and timing of late Cenozoic uplift and tilt of the central Sierra Nevada, California: Evidence from the upper San Joaquin River basin.* Report.

Kanamori H and Hadley D (1975) Crustal structure and temporal velocity change in southern California. *Pure and Applied Geophysics* 113: 257–280.

Katuwal S and Pretell R (2025) Numerical Assessment of V s Profile Gradient as a Site Response Predictor. In: *Proceedings of the Geotechnical Frontiers 2025*. Louisville, KY.

King PB, Beikman HM and Edmonston GJ (1974) *Geologic map of the United States (exclusive of Alaska and Hawaii)*. Report.

Konno K and Ohmachi T (1998) Ground-motion characteristics estimated from spectral ratio between horizontal and vertical components of microtremor. *Bulletin of the Seismological Society of America* 88: 228–241.

Kottke A, Lavrentiadis G, Marafi N, et al. (2025) arkottke/pygmm: v0.8.0 (2025-07-24) (v0.8.0). Zenodo.

Lavrentiadis G, Abrahamson NA and Kuehn N (2021) A non-ergodic effective amplitude ground-motion model for California. *Bulletin of Earthquake Engineering* 21: 5233–5264.

Phillips WS and Stead RJ (2008) Attenuation of Lg in western US using the US Array. *Geophysical research letters* 35(7).

Phillips WS, Mayeda KM, and Malagnini L (2014) How to Invert Multi-Band, Regional Phase Amplitudes for 2-D Attenuation and Source Parameters: Tests Using the US Array. *Pure and Applied Geophysics* 171(3-5): 469–484.

Pinilla-Ramos CI, Abrahamson NA, Marcou S, Dreger DS, Savvaidis A, Atkinson GM, Shelly D, Hassani B, Sung C-H, and Youngs R. Examining the causes of regional differences in California based on ground motions from small-to-moderate earthquakes.

Régnier J, Bonilla LF, Bertrand E, et al. (2014) Influence of the V_S profiles beyond 30 m depth on linear site effects: Assessment from the KiK-net data. *Bulletin of the Seismological Society of America* 104(5): 2337-2348.

Seabold S and Perktold J (2010) Statsmodels: econometric and statistical modeling with python. SciPy 7(1): 92-96.

Thompson EM and Worden CB (2018) Estimating rupture distances without a rupture. *Bulletin of the Seismological Society of America* 108(1): 371-379.

Unruh JR (1991) The uplift of the Sierra Nevada and implications for late Cenozoic epeirogeny in the western Cordillera. *Geological Society of America Bulletin* 103(11): 1395-1404.

Wells DL and Coppersmith KJ (1994) New empirical relationships among magnitude, rupture length, rupture width, rupture area, and surface displacement. *Bulletin of the Seismological Society of America* 84(4): 974-1002.